

Tensile stress regulated microstructures and ferroelectricproperties of $Hf_{0.5}Zr_{0.5}O_2$ films

Siying Huo(霍思颖), Junfeng Zheng(郑俊锋), Yuanyang Liu(刘远洋), Yushan Li(李育姗), Ruiqiang Tao(陶瑞强), Xubing Lu(陆旭兵), and Junming Liu(刘俊明)
Citation: Chin. Phys. B, 2023, 32 (**12**): 127701. DOI: 10.1088/1674-1056/acfb79
Journal homepage: http://cpb.iphy.ac.cn; http://iopscience.iop.org/cpb

What follows is a list of articles you may be interested in

Impact of annealing temperature on the ferroelectric properties of $W/Hf_{0.5}Zr_{0.5}O_2/W$ capacitor

Dao Wang(王岛), Yan Zhang(张岩), Yongbin Guo(郭永斌), Zhenzhen Shang(尚真真), Fangjian Fu(符方健), and Xubing Lu(陆旭兵)
Chin. Phys. B, 2023, 32 (**9**): 097701. DOI: 10.1088/1674-1056/aca9c6

Insight into influence of thermodynamic coefficients on transient negative capacitance in Zr-doped HfO_2 ferroelectric capacitors

Yuan-Yuan Zhang(张元元), Xiao-Qing Sun(孙晓清), Jun-Shuai Chai(柴俊帅), Hao Xu(徐昊), Xue-Li Ma(马雪丽), Jin-Juan Xiang(项金娟), Kai Han(韩锴), Xiao-Lei Wang(王晓磊), and Wen-Wu Wang(王文武)
Chin. Phys. B, 2021, 30 (**12**): 127701. DOI: 10.1088/1674-1056/ac01c4

Improvement of the high-κ/Ge interface thermal stability using an *in-situ* ozone treatment characterized by conductive atomic force microscopy

Ji-Bin Fan(樊继斌), Xiao-Jiao Cheng(程晓姣), Hong-Xia Liu(刘红侠), Shu-Long Wang(王树龙), Li Duan(段理)
Chin. Phys. B, 2017, 26 (**8**): 087701. DOI: 10.1088/1674-1056/26/8/087701

Crystallization behaviors of ultrathin Al-doped HfO_2 amorphous films grown by atomic layer deposition

Xue-Li Ma(马雪丽), Hong Yang(杨红), Jin-Juan Xiang(项金娟), Xiao-Lei Wang(王晓磊), Wen-Wu Wang(王文武), Jian-Qi Zhang(张建齐), Hua-Xiang Yin(殷华湘), Hui-Long Zhu(朱慧珑), Chao Zhao(赵 超)
Chin. Phys. B, 2017, 26 (**2**): 027701. DOI: 10.1088/1674-1056/26/2/027701

Electron trapping properties at HfO_2/SiO_2 interface, studied by Kelvin probe force microscopy and theoretical analysis

Man-Hong Zhang(张满红)
Chin. Phys. B, 2016, 25 (**8**): 087701. DOI: 10.1088/1674-1056/25/8/087701

SPECIAL TOPIC — Post-Moore era: Materials and device physics

Tensile stress regulated microstructures and ferroelectric properties of $Hf_{0.5}Zr_{0.5}O_2$ films

Siying Huo(霍思颖)[1], Junfeng Zheng(郑俊锋)[1], Yuanyang Liu(刘远洋)[1], Yushan Li(李育姗)[1], Ruiqiang Tao(陶瑞强)[1], Xubing Lu(陆旭兵)[1,†], and Junming Liu(刘俊明)[2]

[1] *Institute for Advanced Materials and Guangdong Provincial Key Laboratory of Quantum Engineering and Quantum Materials, South China Academy of Advanced Optoelectronics, South China Normal University, Guangzhou* 510006, *China*

[2] *Laboratory of Solid State Microstructures and Innovation Center of Advanced Microstructures, Nanjing University, Nanjing* 210093, *China*

(Received 26 July 2023; revised manuscript received 12 September 2023; accepted manuscript online 20 September 2023)

The discovery of ferroelectricity in HfO_2 based materials reactivated the research on ferroelectric memory. However, the complete mechanism underlying its ferroelectricity remains to be fully elucidated. In this study, we conducted a systematic study on the microstructures and ferroelectric properties of $Hf_{0.5}Zr_{0.5}O_2$ (HZO) thin films with various annealing rates in the rapid thermal annealing. It was observed that the HZO thin films with higher annealing rates demonstrate smaller grain size, reduced surface roughness and a higher portion of orthorhombic phase. Moreover, these films exhibited enhanced polarization values and better fatigue cycles compared to those treated with lower annealing rates. The grazing incidence x-ray diffraction measurements revealed the existence of tension stress in the HZO thin films, which was weakened with decreasing annealing rate. Our findings revealed that this internal stress, along with the stress originating from the top/bottom electrode, plays a crucial role in modulating the microstructure and ferroelectric properties of the HZO thin films. By carefully controlling the annealing rate, we could effectively regulate the tension stress within HZO thin films, thus achieving precise control over their ferroelectric properties. This work established a valuable pathway for tailoring the performance of HZO thin films for various applications.

Keywords: HfO_2, ferroelectric materials, tension stress, annealing

PACS: 77.55.D–, 77.84.–s, 82.80.Pv, 81.40.Ef **DOI:** 10.1088/1674-1056/acfb79

1. Introduction

In recent years, ferroelectric (FE) HfO_2 thin films have garnered increasing attention owing to their exceptional advantages.[1–4] They exhibit excellent compatibility with the standard CMOS process and possess the ability to maintain robust ferroelectric properties even at the nanoscale, distinguishing them from traditional perovskite ferroelectrics.[5–9] Prior theoretical and experimental research has conclusively demonstrated that the noncentrosymmetric orthorhombic phase (o-phase, *Pca*21) is widely recognized as the fundamental source of ferroelectricity in HfO_2 thin films.[10–12] It has been widely acknowledged that rapid cooling during the annealing process plays a crucial role in the formation of the ferroelectric polar o-phase in FE-HfO_2 films.[13,14] During this annealing process, the doped HfO_2 film is initially heated to a high temperature (usually above 500 °C) to achieve crystallization. Subsequently, the crystalline HfO_2 undergoes a transition from tetragonal phase (t-phase) to o-phase via rapid thermal annealing.[15] However, if a prolonged annealing process is employed, the crystalline film usually experiences a transition from the t-phase to the m-phase, resulting in the absence of polar o-phase in doped HfO_2 film upon cooling down to room temperature.[16,17] The influence of cooling rate during the annealing process on the microstructures and ferroelectric properties of doped HfO_2 films still remains ambiguous. Gaining insight into this aspect would be valuable for a deeper understanding of the origin of the ferroelectricity in doped HfO_2 film.

In this study, we fabricated Zr-doped HfO_2 ($Hf_{0.5}Zr_{0.5}O_2$: HZO) thin films using atomic layer deposition (ALD). The HZO thin films were subjected to annealing with different cooling rates through rapid thermal annealing. The microstructure and electric properties of these HZO films were systematically investigated. The results clearly demonstrated that the cooling rate during the annealing process significantly influences the phase ratio (m/t/o) and stress values in the HZO thin films. We discovered that the variations in phase ratio can be attributed to the intrinsic change in stress within the HZO film, ultimately resulting in distinct ferroelectric properties.

2. Experiments

Figure 1(a) depicts the schematic representation of a W/HZO/W structure fabricated through the following steps. Initially, a W bottom electrode was sputtered onto a Si substrate. Subsequently, HZO thin films were deposited by ALD at 280 °C on the W bottom electrode. $Hf[N(CH_3)_2]_4$, $Zr[N(CH_3)_2]_4$, and O_3 were employed as Hf-precursor, Zr-precursor, and oxygen source, respectively. The Hf:Zr ratio

†Corresponding author. E-mail: luxubing@m.scnu.edu.cn

© 2023 Chinese Physical Society and IOP Publishing Ltd

in the HZO film was estimated to be 1:1. Finally, a W top electrode with a diameter of 100 μm was deposited by sputtering through a shadow mask. The samples then underwent a rapid thermal annealing in a high-purity N_2 atmosphere. The rate of temperature increase during rapid thermal annealing was 30 °C/s. After reaching the desired temperature, the annealing process was maintained at 550 °C for 30 s, followed by cooling at various rates through program control. For the sake of simplicity, the cooling rate during the annealing procedure would be referred to as the annealing rate in the subsequent discussion. The annealing rate without program control (approximately 15 °C/s–18 °C/s), and the sample with programmed annealing rates of 5 °C/s, 3.3 °C/s, 1 °C/s, and 0.5 °C/s were nominated as natural rate, 5 °C/s, 3.3 °C/s, 1 °C/s, and 0.5 °C/s, respectively. The thickness of the HZO thin films was determined by x-ray reflectivity (XRR) measurements. Atomic force microscopy (AFM) was employed to examine the surface morphology of the HZO thin films. The microstructures of HZO thin films were analyzed using grazing incidence x-ray diffraction (GIXRD) and transmission electron microscopy (TEM). Especially, the stress in the HZO thin films was quantitatively determined by the GIXRD $\sin^2\psi$ method.[18–20] The ferroelectric properties and leakage current of the HZO thin films were investigated using a ferroelectric test station (Radiant Precision) and a high-precision semiconductor analyzer (Agilent B1500A).

3. Results and discussion

Figure 1(b) presents the cross-sectional TEM image of the W/HZO/W capacitor structure, showcasing the excellent thickness uniformity of the HZO film deposited via ALD. Notably, the interface between the HZO film and the top/bottom W electrode is distinct, signifying the absence of noticeable interface diffusion. The W top and bottom electrodes exhibit a thickness of approximately 50 nm, while the HZO thin film measures around 15 nm, both closely aligned with the desired thickness control during film growth. XRR measurements are performed to ascertain the thicknesses of the HZO thin films at various annealing rates. Figure 1(c) illustrates a representative XRR curve, from which the thickness of the HZO thin film was determined to be approximately 15 nm, demonstrating an excellent consistency with the TEM result. Figures 1(d) and 1(e) depict the results of the AFM surface topography test for samples annealed at a natural rate and 0.5 °C/s. Upon careful observation, it is found that the sample annealed at the natural rate exhibits a smaller grain size compared to the sample annealed at 0.5 °C/s. Additionally, their RMS values are 732.1 pm and 912.8 pm, respectively. Figure 1(f) summarizes the RMS values of the HZO thin films annealed at various rates, clearly indicating the impact of the annealing rate on the surface morphology of the HZO thin films. As the annealing rate decreases, the surface roughness of the sample progressively increases, reaching its maximum value at 0.5 °C/s. A prolonged annealing process, particularly with an extended cooling time, should be favorable for the nucleation of the grains. Consequently, samples subjected to longer annealing time exhibit bigger grain sizes and, correspondingly, larger RMS values.

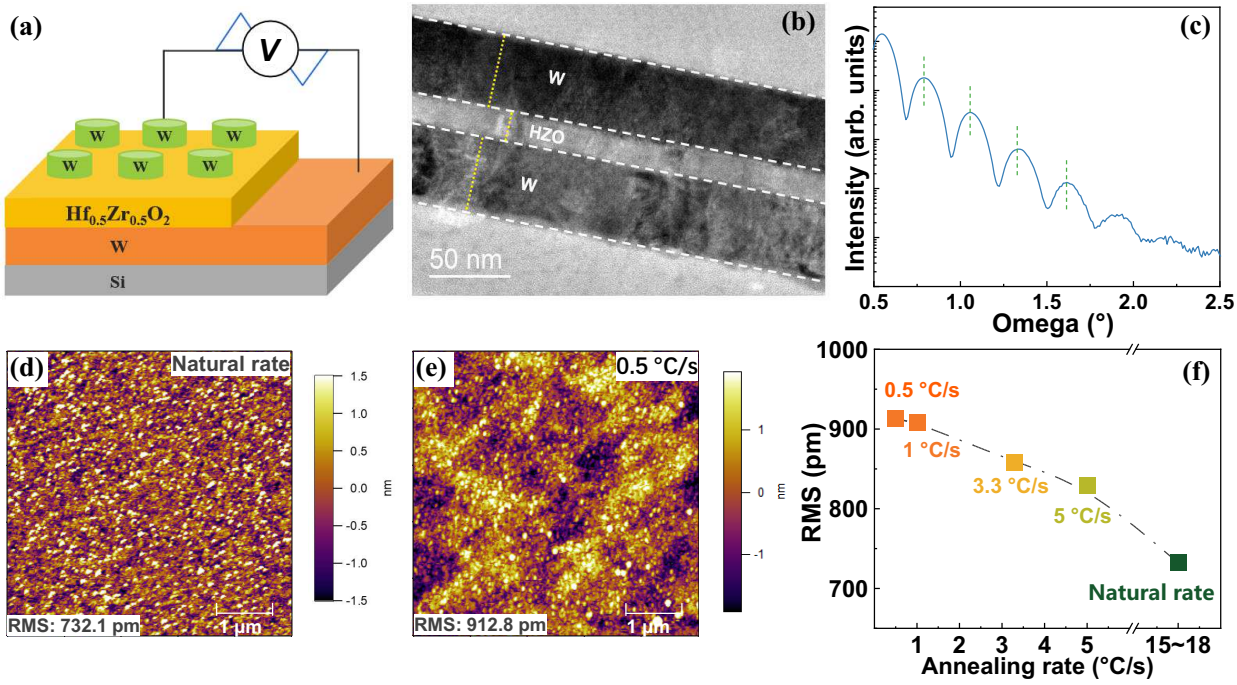


Fig. 1. (a) The schematic diagram of a W/HZO/W capacitor. (b) TEM cross-sectional images of W/HZO/W capacitor. (c) A representative XRR curve of the HZO thin film. (d) AFM measurement result of natural rate HZO thin film. (e) AFM measurement result of 0.5 °C/s HZO thin films. (f) Root of mean square (RMS) values of sample surface morphology with different annealing rates.

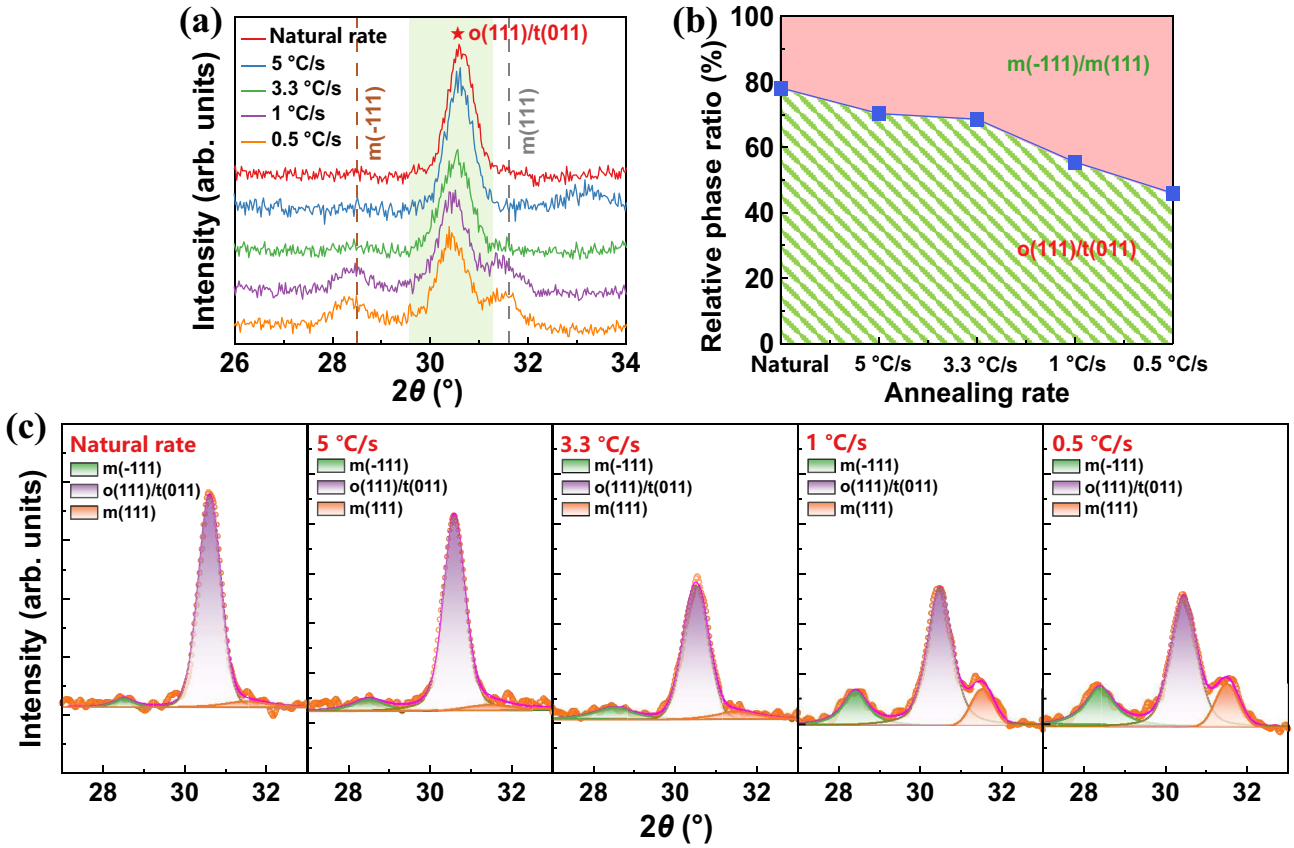


Fig. 2. (a) GIXRD patterns of natural rate, 5 °C/s, 3.3 °C/s, 1 °C/s, and 0.5 °C/s samples. (b) A summary of relative o/t-phase fraction ratio in HZO thin films. (c) Deconvolution results of GIXRD spectra extracted from panel (a).

Figure 2(a) illustrates the GIXRD test results for the samples of natural rate, 5 °C/s, 3.3 °C/s, 1 °C/s, and 0.5 °C/s. The peaks observed at 28.5°, 31.5°, and 30.5° correspond to the m(–111) phase, the m(111) phase, and the mixed peak of ferroelectric o(111) phase and t(011) phase, respectively. Figure 2(b) presents a summary of the phase ratios as a function of the annealing rate, obtained through the deconvolution of the GIXRD patterns illustrated in Fig. 2(a). The detailed deconvolution results are shown in Fig. 2(c). By calculating the area of each deconvoluted phase graph, the relative fractions of the o(111)/t(011) phase and m(–111)/(111) phase for samples with various annealing rates are determined. It is observed that the ratio of the o(111)/t(011) phase decreases as the annealing rate decreases. Specifically, the o(111)/t(011) phase ratios are found to be 78.1% (natural rate), 70.3% (5 °C/s), 68.6% (3.3 °C/s), 55.5% (1 °C/s), and 45.9% (0.5 °C/s), respectively. Conversely, the ratio of m(–111) phase and m(111) phase increases with the decrease in annealing rate. These GIXRD results demonstrate that the polar o-phase and nonpolar m-phase of HZO films can be precisely modulated by adjusting the annealing rate.

Figures 3(a)–3(e) depict the polarization–voltage (*P*–*V*) curves of the HZO thin films with various annealing rates. The curves are obtained by sweeping voltages from 1 V to 6 V at a test frequency of 10 kHz. Upon reaching a scanning voltage of 3 V, ferroelectric hysteresis loops start to emerge, while the *P*–*V* loop tends to become saturated at a scanning voltage of 6 V. Notably, the sample annealed at the natural rate exhibits exceptional ferroelectric properties, with a $2P_r$ value as high as 62.8 μC/cm^2. Figure 3(f) presents a comparison of the *P*–*V* curves for samples annealed at different rates (natural rate, 5 °C/s, 3.3 °C/s, 1 °C/s, and 0.5 °C/s) at a scanning voltage of 6 V (4 MV/cm). As the annealing rate increases, the polarization characteristic curve of the sample gradually contracts and becomes more saturated, exhibiting enhanced ferroelectric properties.

Figure 4(a) presents the $2P_r$ values plotted against the sweeping voltages for all samples with various annealing rates, enabling a direct comparison of their ferroelectric properties. Notably, the $2P_r$ value demonstrates a pronounced voltage dependence, exhibiting an increase with the rise in the scanning voltage. Additionally, at the same scanning voltages, the $2P_r$ value of the HZO thin film exhibits a significant enhancement with increasing annealing rate. These *P*–*V* test results show a good consistency with the GIXRD findings. It is worth highlighting that the sample annealed at the natural rate, with the highest proportion of the o(111)/t(011) phase characterized by GIXRD, possesses the highest $2P_r$ value. Conversely, the sample annealed at 0.5 °C/s, with the lowest ratio of the o(111)/t(011) phase, shows the smallest $2P_r$ value. These re-

sults align well with the notion that the polar o-phase contributes to the ferroelectric behavior of the HfO_2-based ferroelectric films.

Figure 4(b) presents the ε_r–V curves of the HZO thin films annealed at various rates, measured at a scanning voltage of 5 V and a frequency of 1.0 MHz. All of the ε_r–V curves exhibit the characteristic butterfly shape typical of ferroelectric materials, implying excellent ferroelectric properties of the prepared HZO thin films. Additionally, with a decrease in the annealing rate, there is a corresponding reduction in relative permittivity. According to literature reports, the dielectric constant of the t-phase falls within the range of 40 to 50, while that of the ferroelectric o-phase is between 30 and 40, and the m-phase shows a range of 16 to 22. Consequently, we conclude that the slower annealing rate leads to a decrease in the o-phase and an increase in the m-phase in the thin film. This observation aligns with the findings from the GIXRD measurement, providing mutual confirmation of the results.

The fatigue properties of the HZO thin films were investigated using a bipolar triangular pulse wave with a 100 kHz frequency, a 2.5 V polarization reversal voltage, and a 3 V PUND reading voltage. As depicted in Fig. 4(c), samples annealed at the natural rate, 5 °C/s, and 3.3 °C/s exhibited fatigue cycles exceeding 10^8 cycles, whereas samples annealed at 1 °C/s and 0.5 °C/s showed fatigue cycles below 10^8 cycles. The improved fatigue performance of the sample with a faster annealing rate can be attributed to the following mechanisms. Previous studies highlighted the strong correlation between the fatigue properties of HZO thin films and both leakage current and domain pinning effect caused by defects.[21,22] Samples subjected to a faster annealing rate show a smaller grain size and smoother surface roughness, as confirmed by AFM results demonstrated in Figs. 1(d)–1(f). Consequently, the presence of smaller grains and fewer grain boundaries in the film favored lower leakage current. Furthermore, the sample with reduced surface roughness should exhibit better electrode/HZO interface quality, resulting in fewer interface defects and reduced interface domain pinning effects.

Figure 4(d) displays the polarization retention characteristics with time decay, as measured using write/read pulses of 4 V in magnitude and 1 ms in pulse width. The schematic representation of the measurement cycle details can be observed in the inset of Fig. 4(d). Even after a retention time as long as 2×10^4 s, the polarization values of the natural rate, 5 °C/s, 3.3 °C/s, 1 °C/s, and 0.5 °C/s samples remain remarkably high at 91.6%, 96.4%, 97.3%, 84.7%, and 93.7%, respectively. Extrapolating the polarization retention of samples with various annealing rates over a period of 10 years demonstrates the outstanding reliability and retention performance of this HZO thin film.

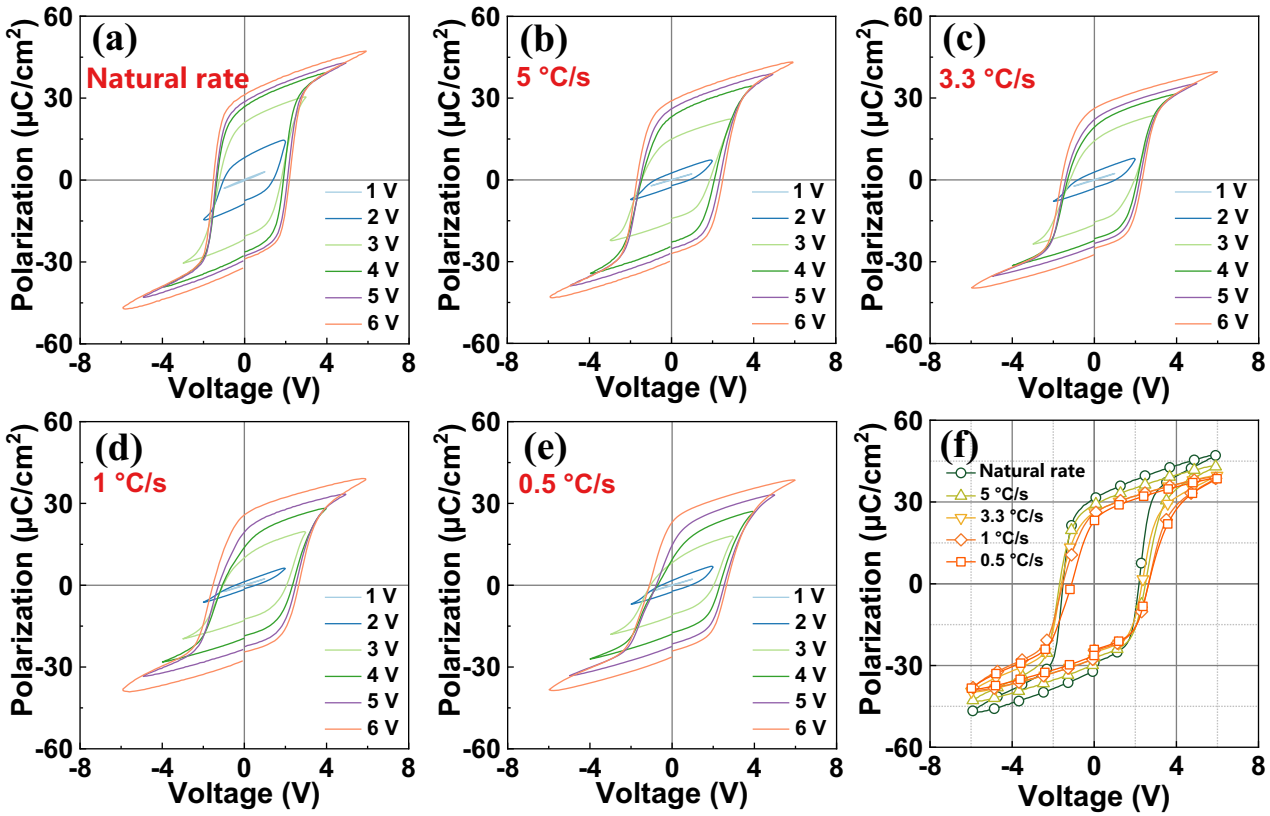


Fig. 3. The P–V hysteresis loops of samples with various annealing rates: (a) natural rate, (b) 5 °C/s, (c) 3.3 °C/s, (d) 1 °C/s, (e) 0.5 °C/s samples. (f) A comparison of P–V hysteresis loops of HZO samples with various annealing rates at a sweeping voltage of ±6 V.

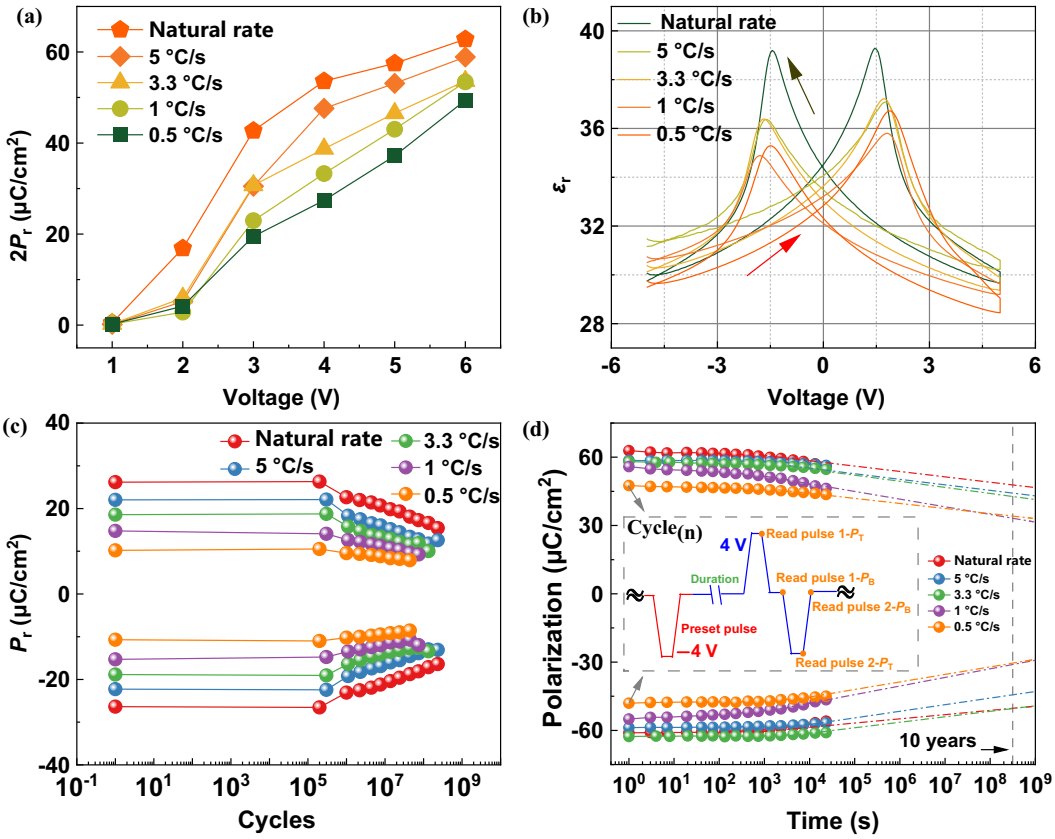


Fig. 4. Comparison of electric properties of HZO thin film samples with different annealing rates. (a) $2P_r$ values under scanning voltage from 1 V to 6 V. (b) Dielectric constant variation with sweeping voltage. (c) Endurance measurement results. (d) Retention properties results. The inset shows pulse details from a single cycle measurement taken during the retention analysis, where P_T and P_B denote the recorded top and bottom polarizations obtained from the read pulses, respectively.

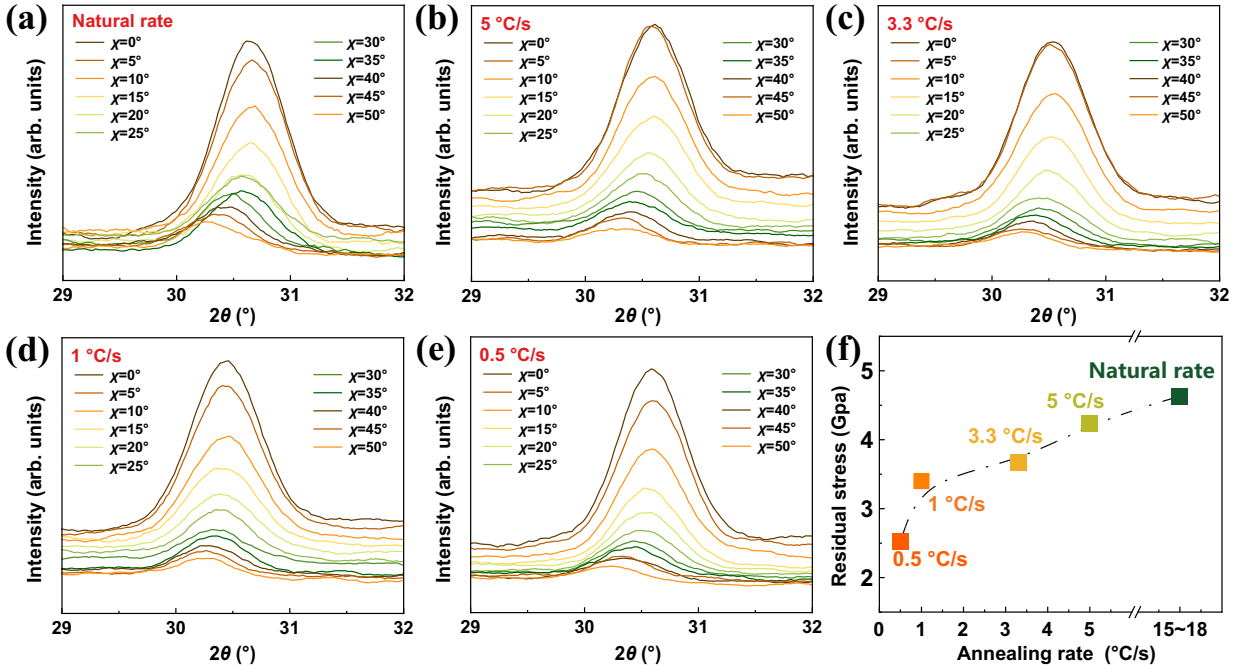


Fig. 5. (a)–(e) GIXRD stress test curves of HZO thin film samples with different annealing rates after 2θ ranging from 29° to 32°. (f) Residual stress values of HZO thin film samples at different annealing rates.

Figures 5(a)–5(e) present the results of GIXRD $\sin^2\psi$ method stress tests conducted on HZO at various annealing rates. In this research, Cu $K\alpha$ rays were used as the ray source, with a 2θ scanning range of 25°–35°, an incident angle of 2°, and a rotation setting range of 0°–50°. As the rotation angle increased from 0° to 50°, a significant reduction in the diffraction peaks of the samples was observed. In addition, the diffraction peak positions displayed a distinct ten-

dency to shift to the left, indicating the presence of tensile stress within the film. Based on the GIXRD $\sin^2\psi$ results, the residual stress values of HZO thin films annealed at different rates were calculated using the method proposed by Zhu *et al.*,[23] as depicted in Fig. 5(f). The residual stresses of the samples annealed at natural rate, 5 °C/s, 3.3 °C/s, 1 °C/s, and 0.5 °C/s were determined to be 4.63 GPa, 4.236 GPa, 3.6715 GPa, 3.4205 GPa, and 2.524 GPa, respectively. All residual stress values fall within the range of 2.5 GPa to 5 GPa, consistent with reported values for HZO thin films.[24] It is evident that the film's residual stress decreases with a lower annealing, demonstrating the significant influence of annealing rate on stress. A faster annealing rate induces larger tension stress in the samples. Notably, stress in the HfO_2-based ferroelectric materials has been reported to critically affect phase stability.[25,26] In this study, a high stress level in the HZO film is assumed to be favorable for the o-phase stability, while low stress favors the stability of the m-phase. Consequently, samples subjected to a faster annealing rate and higher stress have a high ratio of o-phase. Conversely, decreasing stress in the film leads to a reduced o-phase ratio and an increased m-phase ratio. These stress measurement findings provide a reasonable explanation for the distinct microstructure and ferroelectric properties observed in samples with various annealing rates.

4. Conclusion

We explored the influence of tension stress, regulated by the annealing rate during the rapid thermal annealing process, on the microstructure and ferroelectric properties of the HZO thin films. AFM measurements revealed that samples with a faster annealing rate exhibited smaller grain sizes and improved surface roughness. GIXRD measurements indicated precise modulation of the polar o-phase and nonpolar m-phase of HZO films by adjusting the annealing rate, with faster rates leading to a higher o-phase ratio within the film. Electrical measurements indicated that samples with faster annealing rate showed enhanced ferroelectric properties, including higher polarization values and better fatigue cycles. GIXRD stress measurements showed that a faster annealing rate induced larger tension stress in the samples. These findings highlighted the critical role of stress within the HZO films in impacting their ferroelectric properties of HZO thin films.

Acknowledgments

Project supported by the National Natural Science Foundation of China (Grant Nos. 62174059 and 52250281), the Science and Technology Projects of Guangzhou Province of China (Grant No. 202201000008), the Guangdong Science and Technology Project-International Cooperation (Grant No. 2021A0505030064), and the Guangdong Provincial Key Laboratory of Quantum Engineering and Quantum Materials (Grant No. 2020B1212060066).

References

[1] Zagni N, Puglisi F M, Pavan P and Alam M A 2023 *Proc. IEEE* **111** 158
[2] Park J Y, Choe D H, Lee D H, Yu G T, Yang K, Kim S H, Park G H, Nam S G, Lee H J, Jo S, Kuh B J, Ha D, Kim Y, Heo J and Park M H 2023 *Adv. Mater.* **35** 2370312
[3] Banerjee W, Kashir A and Kamba S 2022 *Small* **18** 2107575
[4] Zhang B, Li C L, Hong P Z and Huo Z L 2021 *Appl. Phys. Lett.* **119** 022405
[5] Wei Y F, Matzen S, Quinteros C P, Maroutian T, Agnus G, Lecoeur P and Noheda B 2019 *NPJ Quantum Mater.* **4** 62
[6] Schroeder U, Park M H, Mikolajick T and Hwang C S 2022 *Nat. Rev. Mater.* **7** 653
[7] Ali F, Ali T, Lehninger D, Sunbul A, Viegas A, Sachdeva R, Abbas A, Czernohorsky M and Seidel K 2022 *Adv. Funct. Mater.* **32** 2201737
[8] Cai K M, Yang M Y, Ju H L, Wang S M, Ji Y, Li B H, Edmonds K W, Sheng Y, Zhang B, Zhang N, Liu S, Zheng H Z and Wang K Y 2017 *Nat. Mater.* **16** 712
[9] Zhang B, Meng K K, Yang M Y, Edmonds K W, Zhang H, Cai K M, Sheng Y, Zhang N, Ji Y, Zhao J H, Zheng H Z and Wang K Y 2016 *Sci. Rep.* **6** 28458
[10] Fan S Y, Singh S, Xu X H, Park K, Qi Y B, Cheong S W, Vanderbilt D, Rabe K M and Musfeldt J L 2022 *NPJ Quantum Mater.* **7** 32
[11] Richter C, Schenk T, Park M H, Tscharntke F A, Grimley E D, LeBeau J M, Zhou C Z, Fancher C M, Jones J L, Mikolajick T and Schroeder U 2017 *Adv. Electron. Mater.* **3** 1700131
[12] Huan T D, Sharma V, Rossetti G A and Ramprasad R 2014 *Phys. Rev. B* **90** 064111
[13] Ku B, Choi S, Song Y and Choi C 2020 *IEEE Symposium on VLSI Technology*, June 16–19, pp. 1–2
[14] Gopalan S, Ramesh S, Dutta S and Garbhapu V V 2018 *IOP Conf. Ser.: Mater. Sci. Eng.* **310** 012125
[15] Park M H, Lee Y H, Kim H J, Kim Y J, Moon T, Do Kim K, Hyun S D and Hwang C S 2018 *ACS Appl. Mater. Interfaces* **10** 42666
[16] Lomenzo P D, Takmeel Q, Moghaddam S and Nishida T 2016 *Thin Solid Films* **615** 139
[17] Ho M Y, Gong H, Wilk G D, Busch B W, Green M L, Voyles P M, Muller D A, Bude M, Lin W H, See A, Loomans M E, Lahiri S K and Raisanen P I 2003 *J. Appl. Phys.* **93** 1477
[18] Benediktovitch A, Ulyanenkova T, Keckes J and Ulyanenkov A 2014 *Adv. Mater.* **996** 162
[19] Ma C H, Huang J H and Chen H 2002 *Thin Solid Films* **418** 73
[20] Shi C B, Song Q Z, Wang H, Ma S, Wang C Y, Zhang X, Dou J, Song T L, Chen P W, Zhou H P, Chen Y H, Zhu C, Bai Y and Chen Q 2022 *Adv. Funct. Mater.* **32** 2201193
[21] Peng Y, Xiao W W, Liu Y, Jin C J, Deng X R, Zhang Y Y, Liu F N, Zheng Y Z, Cheng Y, Chen B, Yu X, Hao Y and Han G Q 2022 *IEEE Electron Device Lett.* **43** 216
[22] Lee J H, Chou C H, Liao P J, Chang Y K, Huang H H, Lin T Y, Liu Y S, Nien C H, Hou D H, Hou T H and He J 2022 *IEEE International Electron Devices Meeting (IEDM)*, December 03–07, p. 32
[23] Zhu C, Niu X X, Fu Y H, Li N X, Hu C, Chen Y H, He X, Na G R, Liu P F, Zai H C, Ge Y, Lu Y, Ke X X, Bai Y, Yang S H, Chen P W, Li Y J, Sui M L, Zhang L J, Zhou H P and Chen Q 2019 *Nat. Commun.* **10** 815
[24] Lee S J, Kim M J, Lee T Y, Lee T I, Bong J H, Shin S W, Kim S H, Hwang W S and Cho B J 2019 *AIP Adv.* **9** 125020
[25] Kim S J, Narayan D, Lee J G, Mohan J, Lee J S, Lee J, Kim H S, Byun Y C, Lucero A T, Young C D, Summerfelt S R, San T, Colombo L and Kim J 2017 *Appl. Phys. Lett.* **111** 242901
[26] Lee Y, Goh Y, Hwang J, Das D and Jeon S 2021 *IEEE Trans. Electron Devices* **68** 523